Article

Corresponding Author:
Alvaro Vidal, Department of Mechanical Engineering and Aeronautics, City University of London, Northampton Square, EC1V 0HB London, UK

Email: alvaro.vidal-roncero@city.ac.uk

Modelling of Diesel fuel properties through its surrogates using PC-SAFT

Alvaro Vidal[1]. Carlos Rodriguez[1]. Phoevos Koukouvinis[1]. Manolis Gavaises[1]. Mark A. McHugh[2]

[1]Department of Mechanical Engineering and Aeronautics, City University of London, Northampton Square, EC1V 0HB London, UK

[2]Department of Chemical and Life Science Engineering,
601 West Main Street, Richmond, VA 23284, USA

Abstract

The PC-SAFT equation of state is utilised to model the effect of pressure and temperature on the density, volatility and viscosity of four Diesel surrogates; these calculated properties are then compared to the properties of several Diesel fuels. PC-SAFT calculations are performed using different sources for the pure component parameters. One source utilises literature values obtained from fitting vapour pressure and saturated liquid density data or from correlations based on these parameters (LC-PC-SAFT). The second source utilises a group contribution (GC) method based on the chemical structure of each compound (GC-PC-SAFT). Both modelling methods deliver similar estimations for surrogate density and volatility that are in close agreement with experimental results obtained at ambient pressure. Surrogate viscosity is calculated using the entropy scaling model with a new mixing rule for calculating mixture model parameters. The closest match of the surrogates to Diesel fuel properties provides mean deviations of 1.7% in density, 2.9% in volatility and 8.3% in viscosity. The PC-SAFT results are compared to calculations using the Peng-Robinson equation of state; the greater performance of the PC-SAFT approach for calculating fluid properties is demonstrated. Finally, an eight-component surrogate, with properties at high pressure and temperature predicted with the GC-PC-SAFT method, yields the best match for Diesel properties with a combined mean absolute deviation of 7.1% from experimental data found in the literature for conditions up to 373 K and 500 MPa. These results demonstrate the predictive capability of a state-of-the-art equation of state for Diesel fuels at extreme engine operating conditions.

Keywords: Diesel, surrogates, PC-SAFT, HTHP, modelling

1 Introduction

Improving the combustion efficiency and meeting emission regulations from all types of Diesel powertrains is a pressing environmental issue. Understanding the impact of changes in pressure and temperature on fuel properties is vital for simulating various processes relevant to Diesel injection and combustion. Properties such as density, viscosity, speed of sound and bulk modulus affect the injection process and phase-changing phenomena within the fuel injector, which in turn, control atomisation, mixing, and soot emission levels (1) (2) (3) (4). In addition, recent studies show that injection into air with fuel that reaches supercritical conditions can improve combustion and reduce emissions further (5) (6).

The modelling of Diesel fuel properties in the automotive and energy fields has become a major challenge (7) (8) (9) (10) given the lack of experimental data for the wide range of operating conditions at elevated pressures and temperatures and given the lack of relevant, widely accepted modelling methods/correlations. As Diesel fuel is composed of hundreds of hydrocarbons, with unknown individual properties and interactions, research has focused on creating surrogate mixtures (11) (12) (13) to mimic the properties of Diesel fuel. Surrogate mixtures ideally consist of a rather small number of hydrocarbons that replicate selected properties of a particular Diesel (14). Research with surrogate mixtures could improve the understanding and modelling of the relationships between fuel composition and engine combustion (15).

The modelling of nozzle-cavitation, internal nozzle deposit build-up, fuel atomisation, heating and vaporisation depends on the accuracy of estimated Diesel properties at relevant operating conditions. For example, the recent studies of the author's group (16)

shows an up to 7% variation in the predicted mass flow rate through Diesel injectors when variable fuel properties are utilised. Similarly, considerable effects on nozzle flow and cavitation (17), fuel vaporisation (18) and near-nozzle spray distribution (19) have been demonstrated. The approaches taken by most studies modelling the thermodynamic properties of Diesel fuel are either based on collections of Diesel properties (20), hydrocarbon property databases in NIST (REFPROP (21)), calculated properties using commercially available software, e.g. ASPEN (22) or SUPERTRAPP (23), calculated properties using cubic equations of state (EoS), or a combination of all of these approaches (24). However, there are limitations in each of these approaches. For example, the best collection of Diesel fuel properties (20) is limited to pressures and temperatures far from supercritical or saturated vapour conditions. The REFPROP database is defined for a very limited number of hydrocarbons. In addition, fluid property estimations with software relying on a cubic EoS are known to be inaccurate when calculated at high-temperature, high-pressure conditions (HTHP) (25) (26).

The present study investigates the performance of the Perturbed-Chain, Statistical Associating Fluid Theory (PC-SAFT) (27) equation of state (EoS) for modelling the properties of Diesel fuel and Diesel fuel surrogate mixtures over a wide range of pressure-temperature conditions. The PC-SAFT EoS requires three molecular-based parameters per component for fluid property calculations. In this study two approaches are used to obtain the pure component parameters. One approach utilizes parameters reported in the literature that were obtained by fitting vapour pressure and saturated liquid density data (28) or were calculated with correlations based on parameters reported for compounds in the same chemical family (29) (LC-PC-SAFT). The other approach

utilizes a group contribution method based on the molecular structure of each component (30) in the fuel or fuel surrogate to calculate the three parameters (GC-PC-SAFT). Several advantages accrue when using the PC-SAFT EoS compared to a cubic EoS to calculate fluid properties. The PC-SAFT EoS more accurately predicts derivative properties, reducing errors by a factor of up to eight (31) (32), as compared to predictions with a cubic EoS, such as the Peng-Robinson (PR) EoS (33) or Soave-Redlich-Kwong EoS (34). Density predictions with the PC-SAFT EoS exhibit six times lower error for a widely used surrogate such as dodecane (35) and half the error of those made with improved cubic equations, such as volume-translated versions (36). The PC-SAFT EoS provides satisfactory agreement between calculated and experimental properties of reservoir fluids (37), natural gas (38) and asphaltene phase behaviour (39) (40). These studies suggest the PC-SAFT EoS should provide reasonable predictions of Diesel fuel properties at extreme engine operating pressures and temperatures. Nevertheless, a comparison is provided between properties calculated with the PC-SAFT EoS and those calculated with the PR EoS that demonstrate the superior performance of the PC-SAFT EoS.

Table 1 lists the molecular weights, molar compositions, and normal boiling points of four Diesel surrogates reported by Mueller et al. (41), who refer to the surrogates as V0a, V0b, V1, and V2. The authors of this study group the surrogates into two broad "accuracy" types depending on how closely the composition matches that of a 2007 #2 ULSD certification fuel from Chevron-Phillips Chemical Co. V0a and V0b are labelled low-accuracy surrogates that only contain four and five components, respectively, and V1 and V2 are labelled high-accuracy surrogates that contain eight and nine components,

respectively. V0a, with four components, is derived numerically for combustion and emissions simulations (42). V0b, with five components, better mimics the heavy molecular weight end of the Diesel distillation curve. The authors report that the components in V1 are chosen to match fuel composition, ignition quality, volatility, and density of Diesel (11). V2, the surrogate with the largest number of components, exhibits properties similar to real fuel composition, but it also has five new components with respect to those in surrogate V1. In the present study the PC-SAFT EoS is used to predict the thermodynamic (density and volatility) and transport (viscosity) properties of the four Diesel surrogate mixtures at 0.1 MPa to assess the performance of this EoS to match available surrogate mixture properties. Unfortunately, there are no available experimental literature data for the high-pressure, high-temperature properties of the four surrogates. Therefore, predictions from both the LC-PC-SAFT and GC-PC-SAFT methods are then used to compare calculated surrogate properties to those experimentally reported for Diesel in (11) (41), including high pressure densities and viscosities. The comparison of calculated surrogate mixture properties with experimental Diesel properties provides insight into the impact of the number and type of components needed for a surrogate mixture to mimic Diesel fluid properties.

Compound	M_w [*g*/*mol*]	T_b [*K*]	Surrogate mol % V0a	V0b	V1	V2
n-hexadecane	226.4	560.0	27.8	-	2.7	-
n-octadecane	254.5	590.0	-	23.5	20.2	10.8
n-eicosane	282.5	617.0	-	-	-	0.8
heptamethylnonane	226.4	520.0	36.3	27.0	29.2	-
2-methylheptadecane	254.5	584.3	-	-	-	7.3
n-butylcyclohexane	140.3	456.2	-	-	5.1	19.1
triisopropylcyclohexane	210.4	523.2	-	-	-	11.0
trans-decalin	138.2	460.5	14.8	-	5.5	-
perhydrophenanthrene	192.3	546.9[#]	-	-	-	6.0
1,2,4-trimethylbenzene	120.2	442.6	-	12.5	7.5	-
1,3,5-triisopropylbenzene	204.4	509.5	-	-	-	14.7
tetralin	132.2	480.9	-	20.9	15.4	16.4
1-methylnaphthalene	142.2	518.0	21.1	16.1	14.4	13.9

Table 1:Molar composition for the four Diesel fuel surrogates (V0a, V0b, V1, V2) (41) modelled here. Boiling points at 0.10MPa taken from the literature. [#]: Prediction found in (43)

2 Numerical Method

2.1 PC-SAFT Equation of State

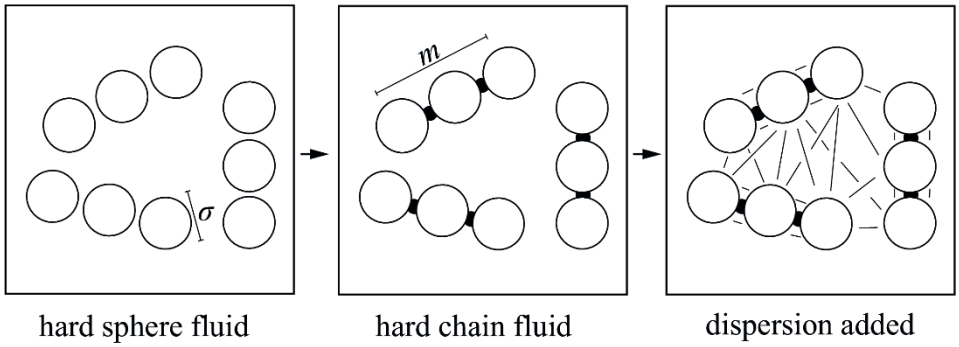

Figure 1:Schematic of three, non-associating molecules modelled with the PC-SAFT EoS. Each molecule is decomposed into spherical segments of diameter σ. The segments then form chains of length m that interact via dispersion forces.

The PC-SAFT EoS (27) is a theoretically derived model, based on perturbation theory (44) (45) (46) (47), that splits the intermolecular potential energy of the fluid into a reference term accounting for repulsive interactions and a perturbation term accounting for attractive interactions. Figure 1 shows the modelling of molecules in PC-SAFT. The reference fluid is composed of spherical segments comprising a hard sphere fluid that then forms molecular chains to create the hard-chain fluid. The attractive interactions, perturbations to the reference system, are accounted for with the dispersion term. Intermolecular interaction terms accounting for segment self- or cross-associations are ignored in the form of the PC-SAFT EoS used here given the molecular structure of the surrogate Diesel compounds listed in Table 1. Hence, each component is characterized by three pure component parameters, which are a temperature-independent segment diameter, σ, a segment interaction energy, ϵ and a number of segments per molecule m.

The PC-SAFT EoS is derived as summations of the residual Helmholtz free energy, as shown in Equation (1).

$$\frac{A^{res}}{RT} = a^{res} = a - a^{ig} = a^{hc} + a^{disp} \#(1)$$

where R is the universal gas constant and T is the temperature. The hard-sphere contribution, a^{hs}, is embedded in the hard-chain term, a^{hc}, which for a mixture of nc components, is given in Equation (2).

$$a^{hc} = \overline{m} a^{hs} - \sum_{i}^{nc} x_i (m_i - 1)\ ln\, g_{ii}^{hs}(\sigma_{ii}) \#(2)$$

where $\overline{m}$ is the number of segments for a multicomponent mixture,

$$\overline{m} = \sum_{i}^{nc} x_i\, m_i \#(3)$$

and x_i is the mole fraction of every component i in the fluid. The hard sphere contribution is defined as

$$a^{hs} = \frac{1}{\zeta_0}\left[\frac{3\zeta_1\zeta_2}{(1-\zeta_3)} + \frac{\zeta_2^3}{\zeta_3(1-\zeta_3)^2} + \left(\frac{\zeta_2^3}{\zeta_3^2} - \zeta_0\right) ln\,(1-\zeta_3)\right] \#(4)$$

where ζ_n are defined abbreviations and the term g_{ij}^{hs} in Equation (5) is the radial distribution function of the hard-sphere fluid.

$$g_{ij}^{hs} = \frac{1}{(1-\zeta_3)} + \left(\frac{d_i d_j}{d_i + d_j}\right)\frac{3\zeta_2}{(1-\zeta_3)^2} + \left(\frac{d_i d_j}{d_i + d_j}\right)^2 \frac{2\zeta_2^2}{(1-\zeta_3)^3} \#(5)$$

where ζ_n is defined as:

$$\zeta_n = \frac{\pi}{6}\rho * \sum_{i}^{nc} x_i\, m_i d_i^n \qquad n \in \{0,1,2,3\} \#(6)$$

and ρ^* is the molecular density and d_i, the temperature-dependent segment diameter of component i is

$$d_i = \sigma_i \left[1 - 0.12\, exp\left(-3\frac{\epsilon_i}{k_B T}\right)\right] \#(7)$$

where k_B is the Boltzmann constant. The dispersion term is defined as:

$$a^{disp} = -2\pi\rho I_1(\eta, \overline{m})\overline{m^2\epsilon\sigma^3} - \pi\rho\overline{m}C_1 I_2(\eta, \overline{m})\overline{m^2\epsilon^2\sigma^3} \#(8)$$

where $\eta = \zeta_3$ is the reduced density, I_1 and I_2 are integrals approximated by simple power series in density, and C_1, an abbreviation for the compressibility factor Z, is given as:

$$C_1 = \left(1 + Z^{hc} + \rho\frac{\partial Z^{hc}}{\partial\rho}\right)^{-1} = \left(1 + \overline{m}\frac{8\eta - 2\eta^2}{(1-\eta)^4} + (1-\overline{m})\frac{20\eta - 27\eta^2 + 12\eta^3 - 2\eta^4}{[(1-\eta)(2-\eta)]^2}\right)^{-1} \#(9)$$

The terms $\overline{m^2\epsilon\sigma^3}$ and $\overline{m^2\epsilon^2\sigma^3}$ are abbreviations which represent properties of the mixture:

$$\overline{m^2\epsilon\sigma^3} = \sum_i^{nc}\sum_j^{nc} x_i\, x_j m_i m_j \left(\frac{\epsilon_{ij}}{k_B T}\right)\sigma_{ij}^3 \#(10)$$

$$\overline{m^2\epsilon^2\sigma^3} = \sum_i^{nc}\sum_j^{nc} x_i\, x_j m_i m_j \left(\frac{\epsilon_{ij}}{k_B T}\right)^2 \sigma_{ij}^3 \#(11)$$

To model the mixture parameters σ_{ij} and ϵ_{ij}, defined for every pair of unlike segments, a modified Berthelot-Lorentz combining rule (48) is used:

$$\sigma_{ij} = \frac{1}{2}(\sigma_i + \sigma_j) \#(12)$$

$$\epsilon_{ij} = \sqrt{\epsilon_i \epsilon_j}\left(1 - k_{ij}\right) \#(13)$$

where k_{ij}, the binary interaction parameter, is used to correct the segment-segment interactions between unlike chains. For the Diesel surrogate mixture compounds listed in Table 1, k_{ij} is expected to be a positive number less than ~0.150 (49) (40). However, in this study k_{ij} is set to zero for predictive calculations that only depend on pure component parameters.

Once the different contributions to the residual molar Helmholtz free energy have been defined, every other thermophysical property can be calculated by its derivatives, as the Helmholtz free energy is a thermodynamic potential. The properties studied in this paper are density, volatility and viscosity.

2.1.1 Method for Calculating Density

At a fixed system pressure *p*, the density of the fluid is adjusted until the calculated pressure equals the system pressure. More specifically, the iterative method uses the packing fraction η and calculates the pressure by the expression

$$p^{calc} = \left(1 + \eta\left[\left(\frac{\partial a^{hc}}{\partial \eta}\right)_{T,x_i} + \left(\frac{\partial a^{disp}}{\partial \eta}\right)_{T,x_i}\right]\right) k_B T \rho^* \, 10^{30} \#(14)$$

Once the iterative method converges, the following expression is used to convert the packing fraction to density in SI units [$\mathrm{kg/m^3}$]:

$$\rho = \frac{6\eta}{\pi}\left(N_{Av}\sum_i^{nc} x_i \, m_i d_i^3\right)^{-1} \sum_i^{nc} x_i M_{w_i}\left(10^{-3}\frac{kg}{g}\right) 10^{30} \#(15)$$

where N_{Av} is Avogadro's number and M_{w_i} is the molar weight in $[g/mol]$ of each component. Details on the derivatives of the residual molar Helmholtz free energy are found in (27).

2.1.2 Method for Calculating Volatility

Volatility, i.e. the conditions governing the formation of vapour in a fluid, is essential to the understanding of bubble formation in injector nozzle flow, to the steps leading to cavitation phenomenon, and, importantly, to the vaporisation of the fuel prior to combustion. In contrast to the behaviour of a pure component, bubble formation within a mixture does not occur at a constant temperature and pressure, but rather each component comprising the Diesel fuel or surrogate mixture vaporises at a different rate dependent on the operating pressures and temperatures. For instance, 1,2,4-trimethylbenzene, the lightest component in several surrogate mixtures, has a boiling point at atmospheric pressure of 442.6 K, but at the same pressure the heaviest component, n-eicosane, boils at 616.9 K. For this study, the occurrence of a vapour bubble in the mixture is determined by minimizing the Gibbs Free Energy and applying the tangent plane criterion to find the most stable state(s) of the fluid system, according to a published algorithm (50) consisting of a stability analysis followed by a phase equilibrium calculation. The stability criterion, i.e. whether the fluid exists as a single phase or as multiple phases, was first proposed by Baker et al. (51), who demonstrated that a fluid system remains a stable single phase for certain conditions of pressure, temperature and composition (here denoted $\boldsymbol{z}$) if the tangent plane to the Gibbs energy surface at composition $\boldsymbol{z}$ is never intersected by the Gibbs energy surface for any other composition $\boldsymbol{x}$. Michelsen (52) provides a mathematical algorithm defining the vertical distance $F(\boldsymbol{x}, T, p)$ from the molar Gibbs energy surface at the trial composition $\boldsymbol{x}$ to the Gibbs energy surface at composition $\boldsymbol{z}$, which in terms of the chemical potential μ_i for every component i is

$$F(\boldsymbol{x}, T, p) = \sum_{i}^{n_c} x_i\big(\mu_i(\boldsymbol{x}, T, p) - \mu(\boldsymbol{z}, T, p)\big) \geq 0 \qquad \forall \boldsymbol{x} \geq 0 \ \#(16)$$

In the present study, Equation 16 is solved using the quasi-Newton BFGS minimization method (53). If $F(\boldsymbol{x}, T, p)$ is negative at molar fraction $\boldsymbol{x}$, the fluid has split into two phases and the phase equilibrium calculation is then solved by searching for the global minimum of the molar Gibbs energy, G, of the system

$$Min\ G = \sum_{i}^{n_c} \sum_{\psi}^{2} n_i^{(\psi)} \mu_i^{(\psi)} \#(17)$$

where $n_i^{(\psi)}$ is the molar number of component i in phase ψ to mole of feed. This minimation problem is also solved with the quasi-Newton BFGS minimization method.

2.1.3 Method for Calculating Viscosity

The recent work by Baled et al. (54) compares the performance of several viscosity models available for hydrocarbons. These authors report that empirical models, such as the Lohrenz-Bray-Clarke (55), are not recommended for high pressure viscosity calculations due to the lack of predictability of the parameters needed in the models. They further note that the semi-theoretical, correlative viscosity prediction methods, e.g. friction theory (56), free volume theory (57) or expanded fluid theory (58), provide satisfactory high pressure viscosity predictions, however these models all require some experimental viscosity data to calculate model parameters. Other semi-theoretical models, popular in reservoir simulations, are the Chung-Ajlan-Lee-Starling (59) and the corresponding states Pedersen and Fredenslund (60) viscosity models, that, unfortunately, fail to provide reliable viscosity predictions at extreme operating conditions. Baled and co-workers recommend using the entropy scaling model of Lötgering-Lin and Gross (61) to calculate viscosity at wide ranges of pressures and temperatures since this model provides predictions in reasonable agreement with experimental data without a need for

fitting parameters. As a consequence of the paucity of experimental data for some of the components used in this work, viscosity will be calculated using the entropy scaling model. These compounds include heptamethylnonane, n-butylcyclohexane, triisopropylcyclohexane and perhydrophenanthrene.

The entropy scaling viscosity model (62) allows transport properties, such as self-diffusion and dynamic viscosity, to be correlated to a power series of the reduced residual entropy, $s^{res}/\overline{m}$, and the universal gas constant, R. For a pure component, the reduced viscosity, μ^*, is obtained with the following expression

$$ln\,(\mu^*) = A_i + B_i\left(\frac{s^{res}}{\overline{m}R}\right) + C_i\left(\frac{s^{res}}{\overline{m}R}\right)^2 + D_i\left(\frac{s^{res}}{\overline{m}R}\right)^3 \#(18)$$

where A_i, B_i, C_i, and D_i are viscosity parameters determined from a specific group contribution method reported by Lötgering-Lin and Gross (61). The reduced viscosity is given by

$$\mu^* = \mu/\mu_{CE} \#(19)$$

where μ_{CE} is the Chapman-Enskog (CE) reference viscosity given as

$$\mu_{CE} = \frac{5}{16}\,\frac{\sqrt{M_w k_B T/(m_{GC} N_A \pi)}}{\sigma_{GC}^2\,\Omega_{GC}^{(2,2)*}} \#(20)$$

where m_{GC} and σ_{GC} refer to the GC parameters and $\Omega_{GC}^{(2,2)*}$ to the reduced collision integral (63).

It is important to recognize that Lötgering-Lin and Gross used the GC method of Sauer, et al. (64) when they developed the viscosity entropy scaling parameters needed for the CE reference viscosity and, therefore, these same GC parameters are used here to calculate the CE viscosity. The Sauer GC parameters differ from those of Tihic, et al.

(30), which are used here for density, volatility, and residual entropy calculations. Tihic's GC parameters provide a better match of the PC-SAFT hexadecane (C16), octadecane (C18), eicosane (C20), and 2-methylheptadecane (2-methyl-C17) pure component parameters found from fitting this EoS to vapour pressure and saturated liquid density data. Rather than fit n-alkane data as a single chemical family, Sauer and co-workers determined n-alkane GC parameters by simultaneously fitting both normal and branched alkane data, which results in ~ 10% lower than expected ε/k values for C16, C18, C20, and 2-methyl-C17. Therefore, in the present study, LC and Tihic's GC-PC-SAFT parameters are used to calculate the residual entropy, Lötgering-Lin and Gross's GC parameters are used to calculate the constants in the entropy scaling equation, and Sauer's GC parameters are used to calculate the CE reference viscosity needed to calculate viscosity. Straightforward mixing rules (65) are used with the PC-SAFT EoS to calculate the fluid properties of the mixtures considered here.

Initial calculations are performed in two different ways to determine, μ_{mix}, the mixture viscosity. One approach uses the Grunberg-Nissan mixing rule (66), which requires values for the viscosity of each component in the mixture

$$ln\,\mu_{mix} = \sum_{i}^{nc} x_i\, ln(\mu_i) + \sum_{i}^{nc}\sum_{j}^{nc}\left(1-\delta_{ij}\right)x_i x_j G_{ij} \quad \#(21)$$

where δ_{ij} is the Kronecker delta, set to 1 when *i=j* and to 0 in any other case. The interaction parameter G_{ij} in the Grunberg-Nissan equation is set to zero here to obtain predictives using only pure component parameters and, in fact, mixture viscosity data is not available to fit this parameter.

where δ_{ij} is the Kronecker delta, set to 1 when *i=j* and to 0 in any other case. The interaction parameter G_{ij} in the Grunberg-Nissan equation is set to zero here to obtain predictives using only pure component parameters and, in fact, mixture viscosity data is not available to fit this parameter.

The second, computationally simpler approach, is to use a mixing rule to calculate A_{mix}, B_{mix}, C_{mix}, or D_{mix} needed to calculate μ^*. The mixing rule used here follows from the mixing rule shown as equation (4) in Novak (65).

$$Z_{mix} = \frac{\sum_i^{nc} x_i m_{i_{GC}} \sigma_{i_{GC}}^2 Z_i}{\sum_i^{nc} x_i m_{i_{GC}} \sigma_{i_{GC}}^2} \#(22)$$

where Z_{mix} stands for A_{mix}, B_{mix}, C_{mix}, or D_{mix}, nc is the number of components in the mixture and x_i is the mole fraction of component i. For each component i, Sauer's GC method (64) is used to calculate $m_{i_{GC}}$, the number of segments, and $\sigma_{i_{GC}}$, the segment diameter. Z_i, which represents A_i, B_i, C_i, or D_i, is calculated using the Lottering-Lin and Gross GC approach for each component.

3 Results and discussion

Initially the PC-SAFT pure component parameters are calculated for the 13 compounds found in the four Diesel fuel surrogates (41), V0a, V0b, V1, and V2, listed in Table 1. Once the pure component parameters are determined, the LC-PC-SAFT and GC-PC-SAFT approach are used to calculate surrogate properties of density, volatility in terms of boiling temperature, and viscosity. These surrogate properties are then compared to available experimental data of the same surrogates (41) available at near ambient conditions and to the properties of six different Diesel fuels (41) (67) at temperatures from 298 to 373 K and pressures from 0.1 to 500 MPa. Unfortunately, there is no

composition characterization information for the five Diesel fuels, those found in (67). Nevertheless, their origin (British), time of year (summer) and existing additives are known, as listed here:

Fuel 1: British refinery #1 with no performance or handling additives.
Fuel 2: British refinery #1 with both handling and performance additives.
Fuel 3: British refinery #2 with both handling and performance additives.
Fuel 4: British refinery #2 with 5% rape methyl ester.
Fuel 5: A commercially available retail fuel.
Fuel 6: A 2007 #2 summer ULSD certification fuel from Chevron-Phillips Chemical Company with detailed compositional analysis (41)

The numerical results are presented in bar graphs, tables, or are interpreted using the Average Absolute Deviation, AAD [%], defined as

$$AAD_{\Omega}[\%] = \frac{100}{N_p}\sum_{i}^{N_p}\left|\frac{\Omega_i^{exp} - \Omega_i^{calc}}{\Omega_i^{exp}}\right| \#(23)$$

where Ω represents the density, boiling temperature, or viscosity and N_p is the number of compared experimental data points.

3.1 LC/GC-PC-SAFT parameter characterization

Parameter	n-Alkanes	Cyclo-Alkanes
m	$0.02569M_w + 0.8709$	$0.02254M_w + 0.6827$
$m\sigma^3$ (Å^3)	$1.7284M_w + 18.787$	$1.7115M_w + 1.9393$
$m\epsilon/k_B$ (K)	$6.8248M_w + 141.14$	$6.4962M_w + 154.53$
Parameter	Aromatics	Branched Alkanes
m	$0.02576M_w + 0.2588$	$0.02569M_w + 0.8709$
$m\sigma^3$ (Å^3)	$1.7539M_w - 21.324$	$(m\sigma^3)_0 / \left(1 + 0.86381\left(\frac{SG}{(SG)_0} - 1\right)\right)$
$m\epsilon/k_B$ (K)	$6.6756M_w + 172.40$	$6.8311M_w + 124.42$

Table 2: Correlations used for the three pure component parameters (29), depending on the hydrocarbon class, when their values were unavailable in the literature. For branched alkanes, the subscript 0 refers to the parameter values for the n-alkane with the same molecular weight as the branched alkane and SG refers to the specific gravity.

The GC-PC-SAFT pure compound parameters are calculated taking into account only the molecular structure (30). In contrast, the LC-PC-SAFT parameters are found in the literature (28) and were obtained by fitting experimental data or were calculated using correlations given in Table 2 for different chemical families (29), when the parameters were not available. The correlations in Table 2 are used to calculate the pure component parameters of 2,2,4,4,6,8,8-heptamethylnonane, 2-methylheptadecane, 1,3,5-triisopropylcyclohexane, perhydrophenanthrene, and 1,3,5-triisopropylbenzene. Table 3 presents the pure component parameters for all 13 components found in different amounts in the four Diesel fuel surrogates considered here.

	LC-PC-SAFT			GC-PC-SAFT		
Palette Compound Name	m	σ[Å]	$\epsilon/k_B[K]$	m_{gc}	σ_{gc}[Å]	$\epsilon_{gc}/k_B[K]$
n-hexadecane	6.6485	3.9552	254.70	6.669	3.944	253.59
n-octadecane	7.3271	3.9668	256.20	7.438	3.948	254.90
n-eicosane	7.9849	3.9869	257.75	8.207	3.952	255.96
heptamethylnonane	6.6883	3.9503	249.88	5.603	4.164	266.46
2-methylheptadecane	7.4090	3.9477	251.44	7.374	3.959	254.83
n-butylcyclohexane	3.6023	4.0637	285.97	3.682	4.036	282.41
1,3,5-triisopropylcyclohexane	5.4251	4.0562	280.40	4.959	4.177	297.48
trans-decalin	3.1578	4.1329	313.21	3.291	4.067	307.98
perhydrophenanthrene	5.0171	4.0410	279.81	4.211	3.851	337.52
1,2,4-trimethylbenzene	3.5204	3.7770	287.45	3.610	3.749	284.25
1,3,5-triisopropylbenzene	5.5241	3.9373	278.21	5.178	4.029	296.68
tetralin	3.3131	3.8750	325.07	3.088	3.996	337.46
1-methylnaphthalene	3.5975	3.8173	335.57	3.422	3.901	337.14

Table 3: LC-PC-SAFT and GC-PC-SAFT pure component parameters for the 13 compounds in the surrogate mixtures listed in Table 1.

The predictive capabilities of the GC and LC models are shown in Table 4 by listing the predicted boiling point at 0.1MPa for each palette component along with the absolute percent deviation from available data. The LC-PC-SAFT predicted boiling points for nine of the palette compounds are within ~ 0.5% of experimental values, while the predictions for heptamethylnonane, 1,3,5-triisopropylcyclohexane, perhydrophenantrene, and 1,3,5-triisopropylbenzene differ by 2-to-9% from experimentally reported values. The reason is not apparent for the larger discrepancy with these four compounds. The performance of the GC-PC-SAFT method is close to, but not quite as good as, that observed with the LC method. For eight palette compounds the error with the GC predicted boiling points are slightly greater than those using the LC method, although the maximum error in these cases is still less than 1.0%. The exceptions are the GC predicted boiling points for the other five palette compounds with the boiling point for 1,3,5-triisopropylbenzene exhibiting a rather large 12.3%. With the exception of the predictions for a few of the

palette compounds, both estimation techniques provide reasonable estimates of the normal boiling temperature without the need for experimental data.

	T_b	Prediction [K]		Error [%]	
Compound	$[K]$	LC	GC	LC	GC
n-hexadecane	560.0	560.0	559.5	0	0.09
n-octadecane	590.0	589.6	590.6	0.07	0.10
n-eicosane	617.0	618.0	620.0	0.16	0.49
heptamethylnonane	520.0	551.5	543.5	6.06	4.52
2-methylheptadecane	584.3	582.0	589.0	0.40	0.80
n-butylcyclohexane	456.2	454.3	453.3	0.42	0.64
1,3,5-triisopropylcyclohexane	523.2	557.0	566.0	6.46	8.18
trans-decalin	460.5	459.3	461.3	0.26	0.17
perhydrophenanthrene	546.9	534.0	569.0	2.36	4.04
1,2,4-trimethylbenzene	442.6	442.0	443.0	0.14	0.09
1,3,5-triisopropylbenzene	509.5	553.5	572.0	8.64	12.3
tetralin	480.9	480.0	481.0	0.19	0.02
1-methylnaphthalene	518.0	516.4	506.4	0.31	2.24

Table 4: Comparison between the experimental normal boiling temperatures, i.e. at 0.1MPa, and the prediction values calculated by LC- and GC-PC-SAFT EoS. The percent errors are equal to $100 \cdot \left|T_{b,calculated} - T_{b,experimental}\right| / T_{b,experimental}$.

3.2 Density

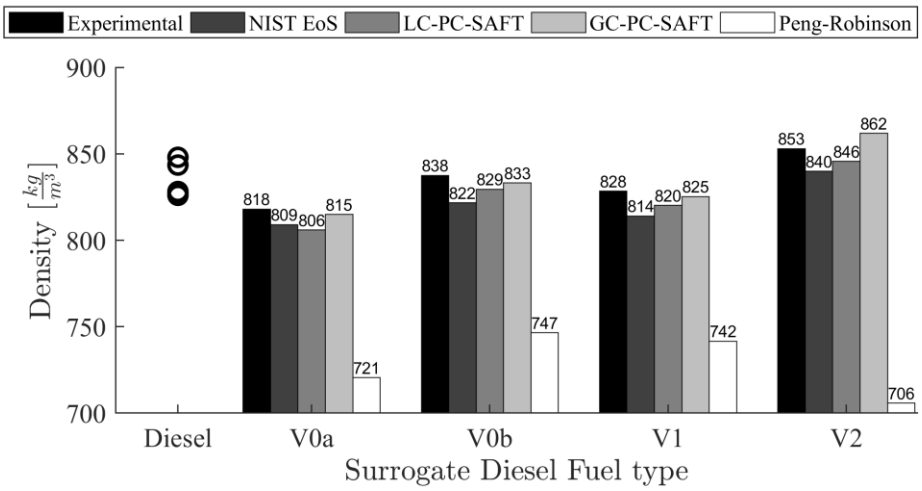

Figure 2: Comparison between experimentally measured surrogate densities at 293 K and 0.1 MPa (41) with predictions made with an EoS-based method developed at NIST (21), the two parameter sets of PC-SAFT and PR EoS. As a reference, the experimental densities of six Diesel fuels at 293K are shown as open circles (41) (67).

Figure 2 shows a comparison between the experimentally measured surrogate densities at 293K and 0.1 MPa with calculated densities using the EoS-based method developed at NIST (21), using the LC- and GC-PC-SAFT modelling methods, and using the widely known PR EoS. As a reference, the open circles in Figure 2 show the experimental densities for the six Diesel fuels (41) (67) at the same condition. Note that the density of Diesel fuels falls into two distinct groups: fuels 1 through 4 originate from refineries and exhibit the lowest densities and fuels 5 and 6, retail and certification fuels, respectively, exhibit higher densities. Overall, the GC-PC-SAFT method gives the closest agreement to surrogate experimental densities, followed by the LC-PC-SAFT method, then the NIST EoS method and lastly, by a large margin, the PR EoS. Table 5 shows the PR EoS pure component parameters used for these calculations. The discrepancies between both PC-SAFT methods with the experimental data are due to the differences in the pure

component and mixture parameters. Nevertheless, at this single temperature and pressure both PC-SAFT calculation methods are within 1.5% of experimental values, with the closest result of 0.37% for the density of V0a. These are strictly predictive calculations since the binary interaction parameters shown in equation 13 are set to zero and, likewise, the binary interaction parameters used in the mixing rules with the PR EoS are also set to zero.

	Peng Robinson parameters			
Compound	$T_c[K]$	$p_c[MPa]$	$\omega[-]$	$Z_c\ [-]$
n-hexadecane	723.0	1.400	0.747	0.241
n-octadecane	747.0	1.290	0.800	0.247
n-eicosane	768.0	1.070	0.876	0.199
heptamethylnonane	693.0	1.570	0.548	0.245
2-methylheptadecane	739.3	1.159	0.727	0.196
n-butylcyclohexane	667.0	2.570	0.534	0.417
triisopropylcyclohexane	685.0	1.653	0.534	0.234
trans-decalin	687.0	3.200	0.274	0.269
perhydrophenanthrene	795.0	2.543	0.554	0.265
1,2,4-trimethylbenzene	649.1	3.200	0.274	0.269
1,3,5-triisopropylbenzene	706.0	1.743	0.554	0.235
tetralin	720.0	3.650	0.304	0.249
1-methylnaphthalene	772.0	3.600	0.348	0.259

Table 5: Properties of pure components within the surrogates for Peng-Robinson EoS. Taken from (68).

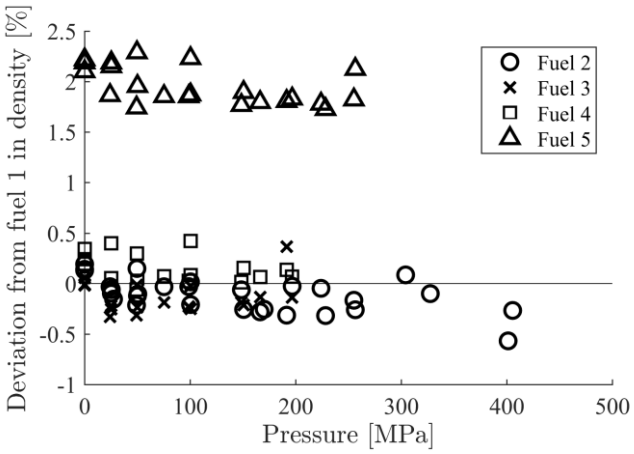

Figure 3: Deviation of the densities of fuels 2 through 5 with respect to the density of fuel 1. These comparisons cover a temperatures from 298 to 373K. The experimental densities exhibit an uncertainty of 0.2% (67). The percent deviations are equal to $100 \cdot (\rho_{fuel\ i} - \rho_{fuel\ 1})/\rho_{fuel\ 1}$.

Unfortunately, high pressure surrogate mixture densities are not available for comparison to the densities of the fuels. However, before comparing calculated and experimental high-pressure fuel densities, it is worthwhile comparing experimental densities of fuels 1 through 5 to ascertain which fuel densities can be grouped and which ones should be considered separately. Figure 3 shows the deviation of the experimental densities of fuels 2 through 5 with respect to the experimental density of fuel 1. The reported experimental uncertainty is 0.2% for all these five fuels. The densities of fuels 1 through 4 agree with one another to within 1.0% while the densities for fuel 5 consistently vary by ~2% regardless of the temperature. Therefore, fuels 1 through 4 will be considered collectively as a single group and fuel 5 will be considered on its own.

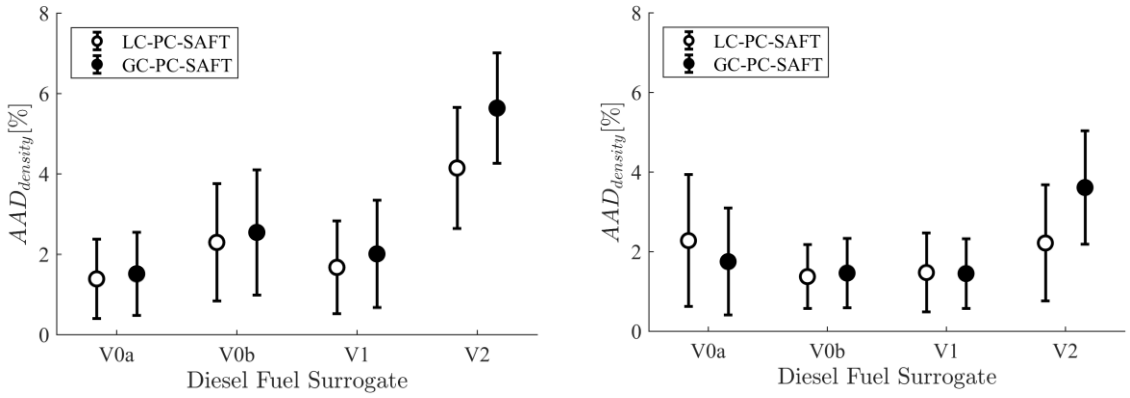

(a) Fuels 1 – 4 (b) Fuels 5

Figure 4: Average Absolute Deviation (AAD) showing the comparison of LC and GC-PC-SAFT predicted densities of the four surrogates with the fuel densities (67) for temperatures from 298 to 373 K and pressures from 0.1 to 500 MPa. Error bars represent one standard deviation.

The LC and GC-PC-SAFT methods are used to predict the densities of the four surrogate mixtures at 298, 323, 348, and 373 K and pressures from 0.1 to 500 MPa, conditions similar to those used to measure densities of fuels 1 through 5 (67). As the NIST-based EoS is unavailable and the Peng-Robinson EoS significantly underperforms in predictions, both are not taken into account for the rest of this section. Figure 4 shows AAD values for the experimental densities of the fuels compared to predicted surrogate densities. The densities of fuels 1 through 4 are, overall, better predicted with the LC-PC-SAFT than the GC-PC-SAFT method. The closest agreements are found with the LC-PC-SAFT method with surrogates V0a (1.5%) and V1 (1.8%). The AAD values for fuels 1 through 4 are all less than 8% for the remaining comparisons of the LC- and GC-PC-SAFT methods and surrogates. Interestingly, both methods match the density of fuel 5 equally well. The largest AAD values for all five fuels are found with calculated densities

of surrogate V2 regardless of the parameter set used for the calculation. Nevertheless, overall, none of the surrogate calculated densities results in an AAD larger than ~6%.

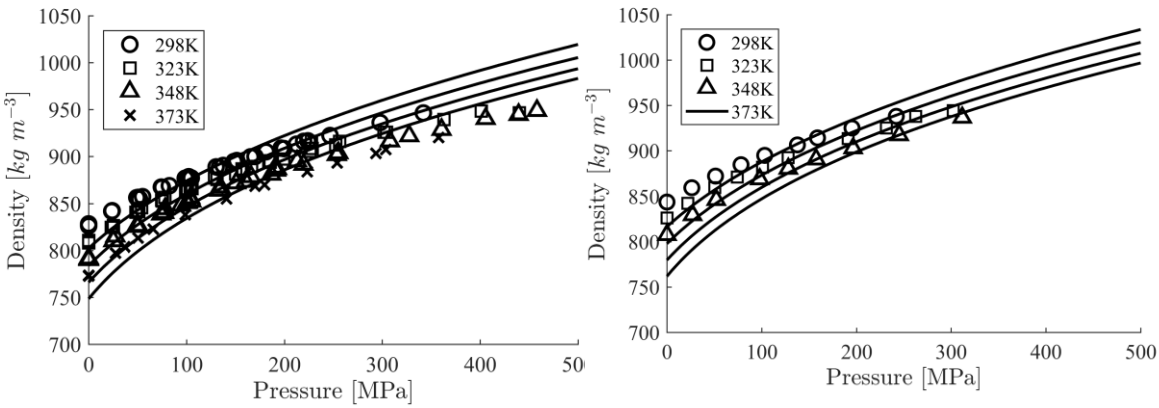

(a) V0a (LC-PC-SAFT) against Fuels 1-4

(b) V1 (LC-PC-SAFT) against Fuel 5

Figure 5: Surrogate densities calculated with LC-PC-SAFT (lines) compared to experimental densities (symbols) (67).

Figure 5 shows a comparison of predicted surrogate densities with experimental fuel densities of (a) fuels 1 through 4 against densities for V0a calculated with the LC-PC-SAFT method and (b) fuel 5 (67) against densities for V1 also calculated with the LC-PC-SAFT method. Plots for the other surrogates and parameter sets are found in the Supporting Information document. For both cases, the predicted surrogate densities are slightly lower than the Diesel densities at all temperatures at low pressures and greater than the Diesel densities at all temperatures at high pressures. This trend is observed regardless of the chosen surrogate. Nevertheless, the maximum deviations are less than 4% at the upper limit of the pressure. However, the greatest discrepancy noted in these comparisons is that slopes of the predicted isotherms are not in agreement with the slopes of the experimental data. Hence, predicted isothermal compressibility will be in significant disagreement with experimental values.

3.3 Volatility

Figure 6 shows the predicted volatility curve at 0.1MPa for all four surrogates, calculated with LC-, GC-PC-SAFT and PR EoS, against the experimental curves for both the surrogates and fuel 6. It is obvious that PR EoS estimations are in greater disagreement with experimental data than both methods of PC-SAFT. As expected, the boiling temperatures increase with increasing vapour fraction as heavier hydrocarbons remaining in the liquid phase require more energy and, hence, higher temperatures, to vaporise.

At vapour fractions up to ~10% the PC-SAFT approach, with either method used to calculate pure component parameters, overpredicts the surrogate boiling temperatures by as much as $5^{o}C$ while at vapour fractions greater than 60% this model underpredicts boiling temperatures. At vapour fractions greater than 80%, estimations for the "high accuracy" surrogates are a very poor match, where the deviation is close to $40^{o}C$ at a vapour fraction of 90%.

Similar conclusions are evident for the comparison of calculated surrogate vapour fractions with those for fuel 6, where a significant error close to complete vaporisation is also observed.

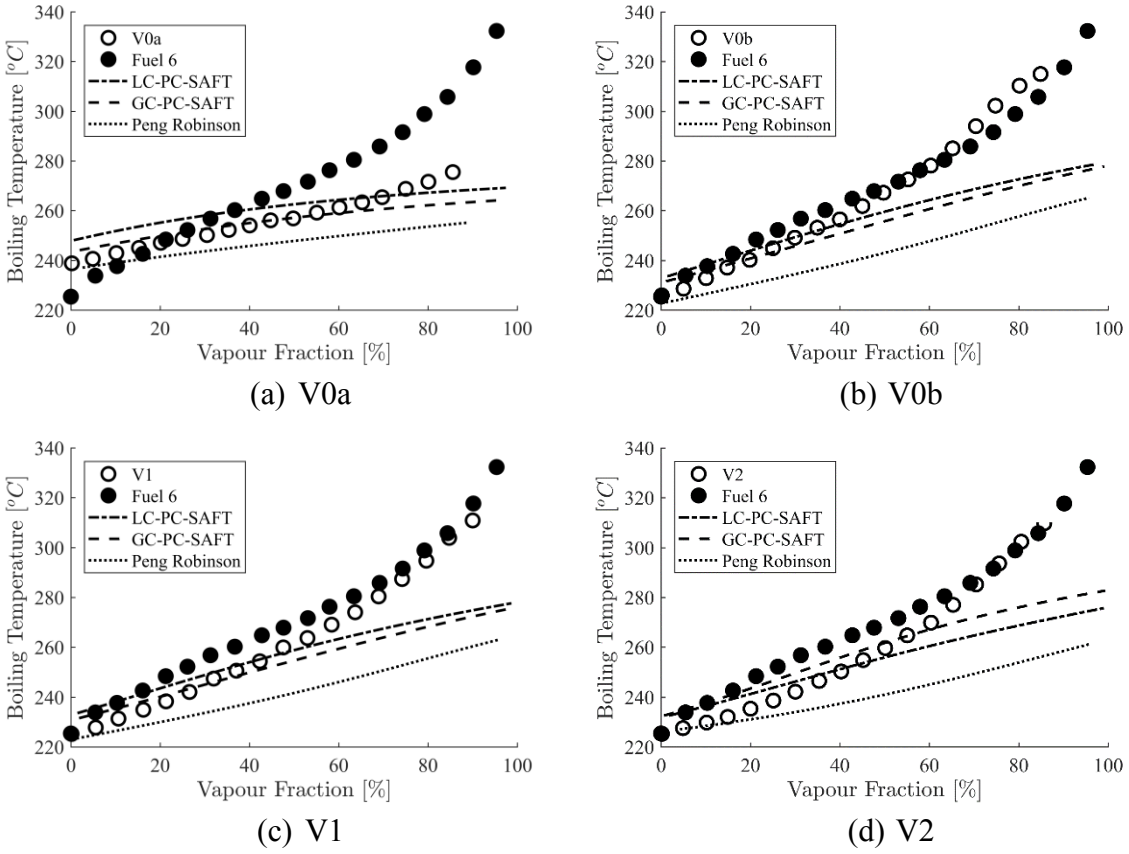

Figure 6: Volatility curves at 0.1MPa predicted by the PC-SAFT and PR EoS compared to experimental data for both surrogates and Fuel 6.

Figure 7 presents *AAD* values for experimental volatility curves at a constant pressure of 0.1 MPa for the four Diesel fuel surrogates (41) and that of fuel 6 (41), compared to predictions using the LC-PC-SAFT and GC-PC-SAFT methods, i.e. *AAD* values for the results shown in Figure 6. Peng-Robinson estimations are omitted as they are clearly in greater disagreement than those of PC-SAFT. Both PC-SAFT parameter sets provide very similar boiling temperature estimates in close agreement to experimental values for all four surrogates, as shown in Figure 7a, particularly for V0a (1.4 - 2.3%).

The comparison against real Diesel volatility, Figure 7b, shows the LC-PC-SAFT estimates using V0b (5.9%), V1 (6.2%) and V0a (6.3%) are closer to experimental values than those obtained with the GC method. Conversely, the GC-PC-SAFT estimates using V2 (5.3%) are closer to real Diesel data than those obtained with the LC method. Overall, the averaged errors for all surrogates by either method are within ~10% of the observed values.

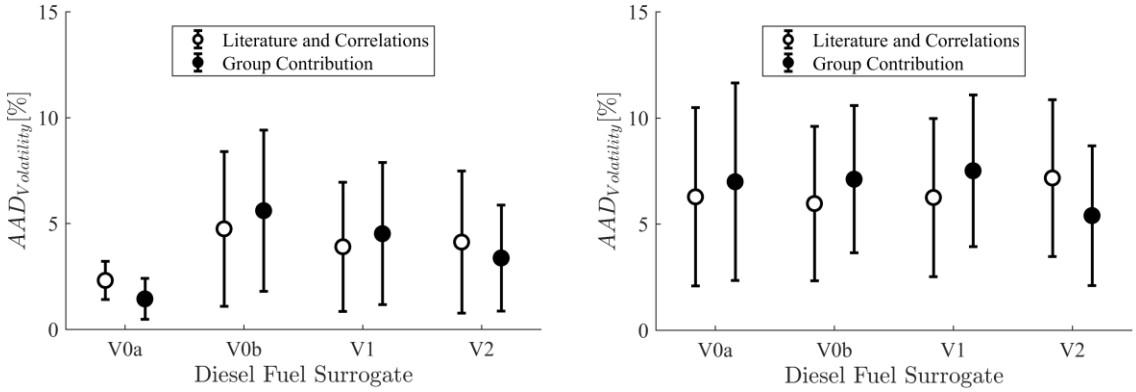

(a) Against surrogate data (b) Against Diesel data

Figure 7: Average Absolute Deviation ($AAD_{Volatility}$) for experimental boiling temperatures of four surrogates and Fuel 6 (41) at 0.1 MPa with predictions using the LC-PC-SAFT and GC-PC-SAFT calculation methods. Error bars represent one standard deviation.

3.4 Viscosity

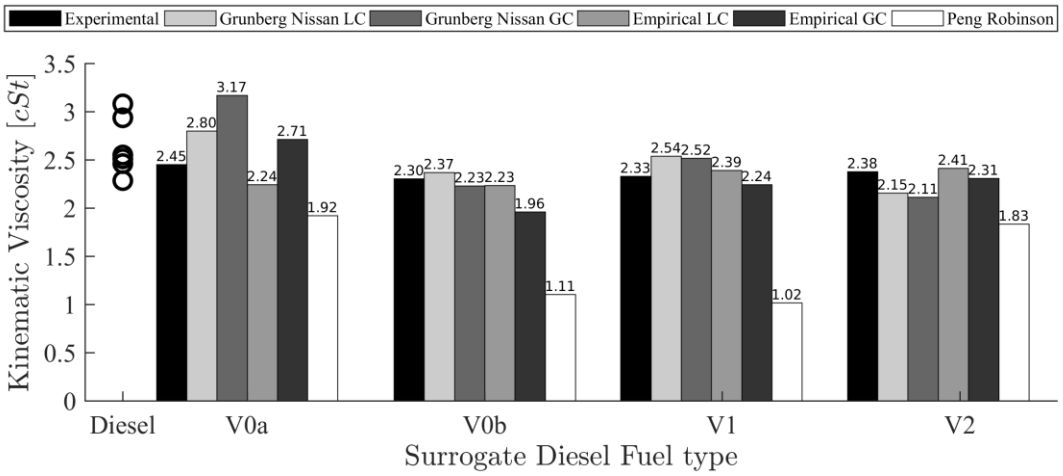

Figure 8: Comparison of experimental kinematic viscosities of four surrogates at 313.15 K and 0.1 MPa (41) to predictions using PC-SAFT with both parameter sets and mixing rules, and Peng Robinson (69). As a reference, the open circles show the experimental kinematic viscosities of the six Diesel fuels at the same condition (67) (41) considered in this study. Units: 1cSt=10^{-6} m^2 s^{-1}

Figure 8 presents a comparison of experimental kinematic viscosity at 0.1 MPa and 313 K for the four surrogates (41) to those estimated by PR (69) and the PC-SAFT with both the LC and GC pure component parameters. Mixture viscosities are calculated with PC-SAFT using both the empirical (EM) mixing rule in Equation (22) and the Grunberg-Nissan (GN) mixing rule in Equation (21). On the other hand, only GN is applied to PR-EoS estimations in absence of any better alternative. For most cases the GC-PC-SAFT model with the EM mixing rule gives the closest predictions to surrogate experimental values with errors of 8.6% for V0a, 2.6% for V1, and 1.5% for V2. Predictions of the V0b kinematic viscosity with either the LC or GC-PC-SAFT method with the EM mixing rule give similar matches to the experimentally observed value. Peng-Robinson fails to provide accurate estimations, with errors ranging 20 to 60%. Thus, the results provided

by the Peng-Robinson EoS are omitted in the rest of this section. Moreover, overall viscosity predictions using the empirical mixing rule shown in Equation (22) provide slightly better matches with experimentally-observed values compared to predictions using the Grunberg-Nissan (GN) mixing rule, Equation (21). While it is possible to adjust the GN rule with a mixture-specific correction factor (66), this was not done to maintain fidelity with the decision to set binary interaction correction factors to zero in the PC-SAFT EoS mixing rules. Given that the empirical mixing rule, Equation (22), is computationally easier to use compared to the GN rule, the remaining mixture viscosity calculations are done with the EM mixing rule.

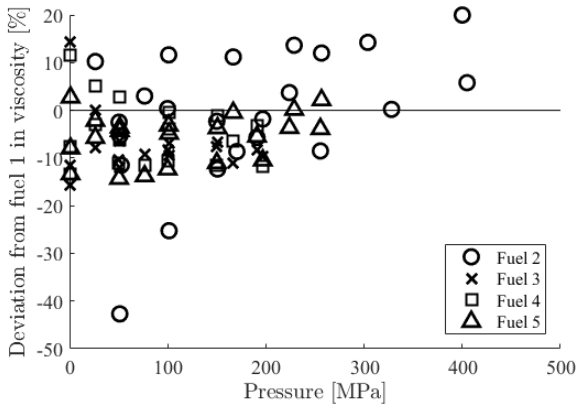

Figure 9: Deviation in viscosity of fuels 2 through 5 relative to the viscosity of fuel 1 (67). These comparisons cover a temperature from 298 to 373K. The uncertainty in the experimental viscosity is 2%. The percent errors are equal to $100 \cdot (\mu_{fuel\,i} - \mu_{fuel\,1})/\mu_{fuel\,1}$

Before comparing calculated and experimental high-pressure fuel viscosities, it is worthwhile comparing experimental viscosities of fuels 1 through 5 to ascertain which fuel viscosities can be grouped and which ones should be considered separately, similar to the analysis performed with the fuel density data. Figure 9 shows a deviation plot comparing the viscosity of fuel 1 to the viscosity of fuels 2 through 5. The reported

experimental uncertainty is 2%. The bulk of the viscosity data deviation for the different fuels falls within a range of ± 15%, which is much larger than the experimental uncertainty in the data. The large variation in viscosities is likely a consequence of the use of additives in fuels 2 through 5. Interestingly, these additives have very little effect on the density of the fuels as previously shown in Figure 3. Note that additised fuel 2 exhibits the highest deviations and, therefore, the viscosity of fuel 2 is compared separately to the viscosity of the surrogates.

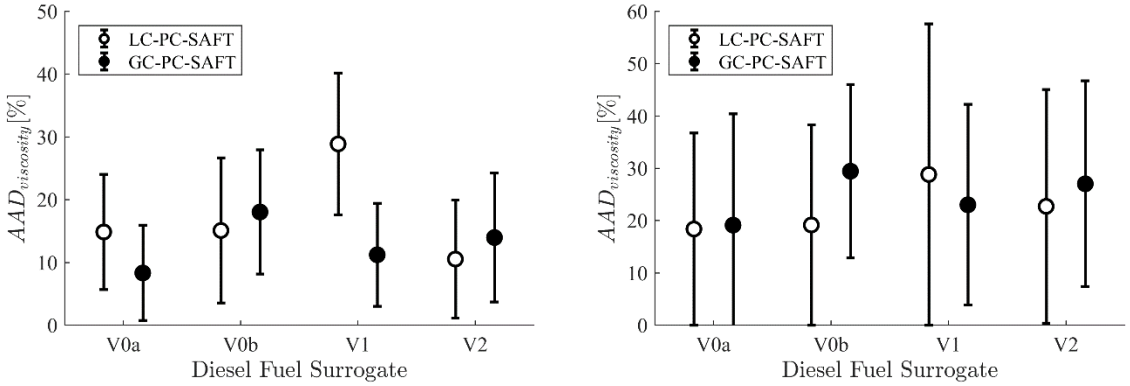

(a) Fuels 1, 3, 4, and 5 (b) Fuel 2

Figure 10: Average Absolute Deviation (*AAD*) showing how closely the entropy scaling predicted viscosities of the four surrogates match experimental viscosities averaged from Diesel fuels (67) for temperatures from 298 to 373 K and pressures from 0.1 to 500 MPa. The predictions use the empirical mixing rule defined in equation 21. Error bars represent one standard deviation.

Figure 10 compares dynamic viscosities averaged from fuels 1, 3, 4, and 5 (10a) and from fuel 2 (10b) (67) obtained at 298, 323, 348, and 373 K and pressures from 0.1 to 500 MPa to predicted surrogate viscosities over the same temperature-pressure ranges. Similar to the comparison of kinematic viscosity at low pressure, both parameter sources give similar predictions, with the exception of V1 calculated with LC-PC-SAFT. As shown, the errors for fuel 2 are greater than those for the other fuels, and in many cases the errors for fuel 2 are twice as large.

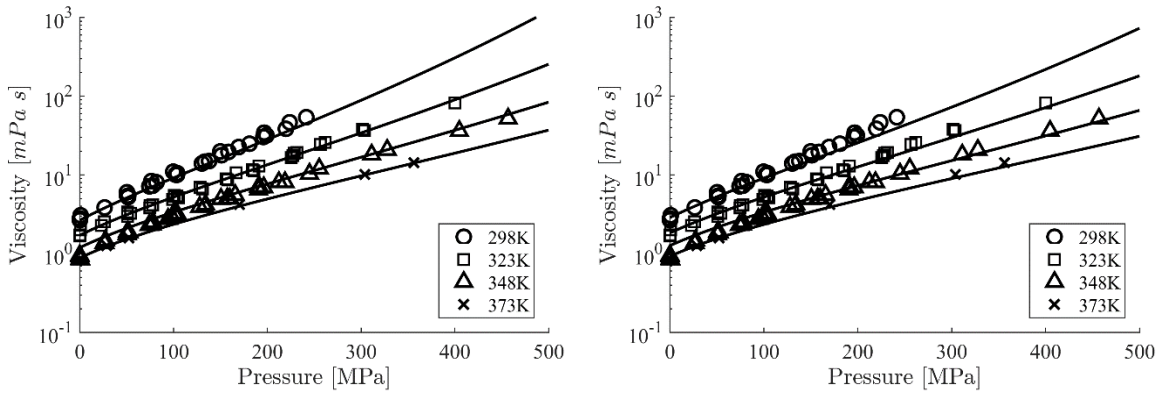

(a) V0a (GC-PC-SAFT) (b) V2 (LC-PC-SAFT)

Figure 11: Comparison of averaged experimental viscosities for fuels 1, 3, 4, and 5 (67) to those predicted by PC-SAFT. The calculation uses the empirical mixing rule defined in equation 21.

A detailed viscosity comparison is provided in Figure 11 which shows predictions for V0a (GC-PC-SAFT) and V2 (LC-PC-SAFT) against averaged experimental data for fuels 1, 3, 4, and 5 (67). Plots for the other surrogates and both parameter sources are found in the Supporting Information document. Both the predicted and experimental viscosities increase with increasing pressure although the rate decreases as temperature increases. The predicted surrogate viscosities are in reasonably good agreement with experimental values for these retail Diesel fuels at most conditions. The largest increase in viscosity observed experimentally is at low temperatures and high pressures. It is in this region, at 298 K, where the disagreement between data and prediction is as high as 15%. This mismatch in viscosities at low temperatures and high pressures is characteristic of most viscosity models (36).

3.5 Discussion

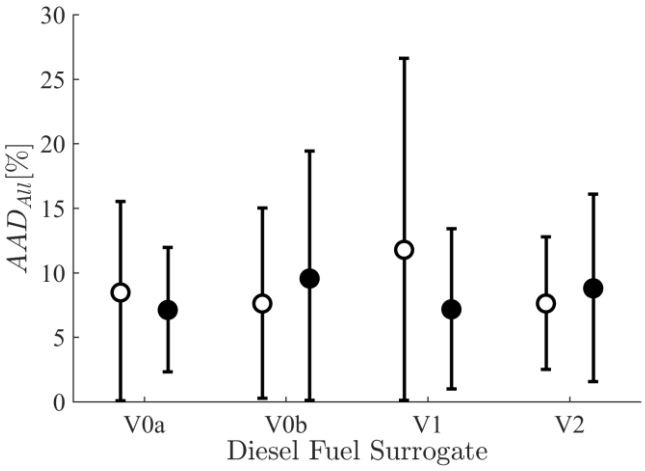

Figure 12: Average Absolute Deviation (AAD_{all}) showing the performance of four different surrogates to match the combined set of density, volatility, and viscosity data for six different Diesel fuels at temperatures from 298 to 373 K and pressures from 0.1 to 500 MPa. Error bars represent one standard deviation.

Although it is possible to match each thermodynamic property of Diesel fuel with a unique surrogate mixture, the normal practice is to use a small number of surrogate mixtures, if not just one mixture, to mimic all of the properties of a Diesel fuel. Figure 12 shows an assessment of how closely a combined set of Diesel fuel density, volatility, and viscosity data for six different Diesel fuels (67) (41) at 298 to 373 K and 0.1 to 500 MPa match with each surrogate mixture considered in this study. For the calculation of these errors, each property contributes in the same amount to the total error. When a combined set of Diesel fuel properties are considered, it is evident that neither modelling option considered in this study is favoured. The lowest AAD_{all} is found for surrogate V1 (GC-PC-SAFT calculations) (7.1%), followed by V0a (GC-PC-SAFT calculations) (7.1%) and V2 (LC-PC-SAFT calculations) (7.6%) . AAD_{all} values for the rest of predictions, although larger, are still less than ~10% with the exception of V1 (LC-PC-SAFT calculations) with a deviation of ~11.7%.

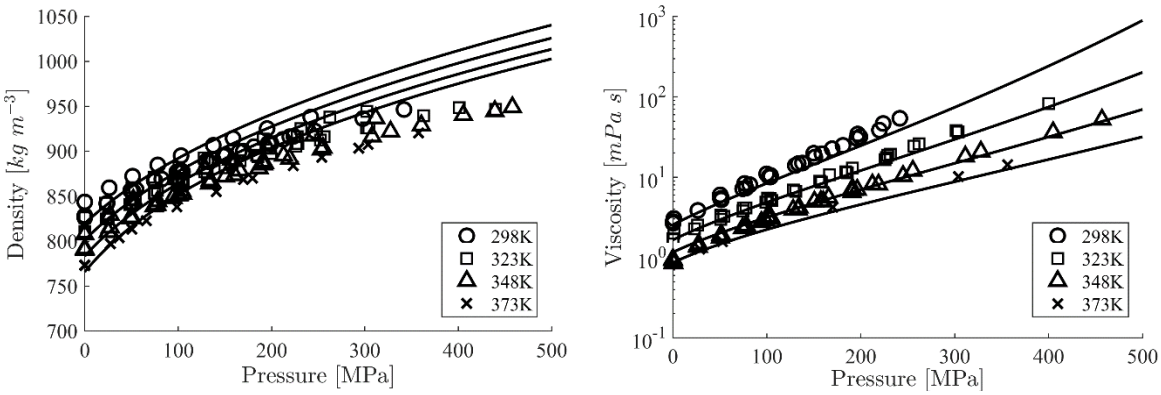

(a) Density (b) Viscosity

Figure 13: Isotherms for surrogate V1 calculated with the GC-PC-SAFT method compared to experimental data for Diesel fuels 1 through 6.

The combined GC-PC-SAFT predicted properties for the V1 surrogate had the best match to the studied Diesel fuel properties. Figure 13 (a) and (b) show how well the predicted V1 properties match the densities and viscosities of fuels 1 through 6. As shown in Figure 13 (a), the observed averaged Diesel density is underpredicted at low pressures and overpredicted at high pressures. However, these errors are within a maximum of ~3%. For viscosity, although it should be largely better than PR EoS, there is an important underprediction at low temperatures with errors as high as ~15%. Regarding volatility, as shown previously in Figure 6, the predictions overestimate the data at low vapour fractions and underestimate the data at high vapour fractions, with a maximum deviation of ~40 ^{o}C at a vapour fraction of 95%.

4 Conclusions

The properties of four surrogates proposed by Mueller, et al. (41) were modelled using the PC-SAFT EoS to test the performance of this model to predict density, volatility, and viscosity. The PC-SAFT pure component parameters for the compounds in each

surrogate mixture were obtained either from the literature or were calculated using correlations based on literature parameters (LC-PC-SAFT) or were calculated using a group contribution method (GC-PC-SAFT). Predicted surrogate mixture properties were then compared to available property data for Diesel fuels. Both methods provided good predictions for the densities of the four surrogate mixtures. Likewise, the predicted surrogate mixture densities were in reasonably close agreement with Diesel fuel density reported over broad temperature and pressure ranges. Both methods also exhibited similar deviations for predicted normal boiling points for the surrogates and both methods exhibited similar trends in the distillation curves where predicted temperatures were too high at low vapour fractions and too low at high vapour fractions. High temperature, high pressure predicted surrogate viscosities obtained with the entropy scaling viscosity model matched Diesel experimental data (67) within ~15% when using either the LC and GC parameter estimation techniques. Comparisons are also presented for calculations with both the PC-SAFT and PR EoS, showing the greater performance of the PC-SAFT EoS. Overall, the V1 surrogate modelled with the GC-PC-SAFT method provided the best match of Diesel properties when a combination of Diesel properties was considered. These results demonstrate the predictive capability of a state-of-the-art equation of state for Diesel fuels at extreme operating conditions.

Acknowledgements

This project has received funding from the European Union Horizon-2020 Research and Innovation Programme. Grant Agreement No 675528. The authors thank several of the members of Professor Gross's research group for helpful technical advice on the application of the entropy scaling technique for calculating viscosity.

List of symbols

English symbols

a	reduced molar Helmholtz free energy	k_{ij}	binary interaction parameter
A	molar Helmholtz free energy	m	chain segment number
A_{mix}	mixture viscosity parameter	$\overline{m}$	mean chain segment number
B_{mix}	mixture viscosity parameter	M_w	molar weight
C_{mix}	mixture viscosity parameter	N_{Av}	Avogadro's number
C_1	defined abbreviation (Eq. 9)	n	number of moles
d	temp. dependent segment diameter	p	pressure
D_{mix}	mixture viscosity parameter	R	universal gas constant
g_{ij}	site-site radial distribution function	s	entropy
G_{ij}	viscosity binary interaction parameter	T	temperature
G	Gibbs free energy	X	generic viscosity parameter
k_B	Boltzmann constant	Z	compressibility factor

Greek symbols

ϵ	depth of the potential	ρ^*	molecular density
ζ_n	defined abbreviation (Eq. 6)	ρ	mass density
η	packing fraction	σ	segment diameter/standard deviation
μ^*	reduced viscosity	Ω	reduced collision integral or

			generic
μ	dynamic viscosity or chemical pot.		thermodynamic property
ψ	generic phase	ω	acentric factor

Superscripts

disp	dispersion term	*ig*	ideal gas
hc	hard-chain term	*res*	residual term
		hs	hard-sphere term

Subscripts

i	component *i* or the *i*th data point	*a*	attractive contribution
GC	group contribution parameter	*r*	repulsive contribution
mix	mixture property	c	Critical property

Abbreviations

%*AAD*	average absolute deviation
EoS	equation of state
GC-PC-SAFT	group contribution PC-SAFT
LC-PC-SAFT	literature and correlations PC-SAFT
PC-SAFT	perturbed chain statistical associating fluids theory
nc	number of components
GN	Grunberg-Nissan mixing rule
EM	empirical mixing rule

References

1. Tat ME, Van Gerpen JH, Soylu S, Canakci M, Monyem A, Wormley S. The speed of sound and isentropic bulk modulus of biodiesel at 21 C from atmospheric pressure to 35 MPa. Journal of the American Oil Chemists' Society. 2000; 77: p. 285–289.
2. Hoekman SK, Robbins C. Review of the effects of biodiesel on NOx emissions. Fuel Processing Technology. 2012; 96: p. 237–249.
3. Lapuerta M, Armas O, Rodriguez-Fernandez J. Effect of biodiesel fuels on diesel engine emissions. Progress in Energy and Combustion Science. 2008; 34: p. 198–223.
4. Wei M, Li S, Xiao H, Guo G. Combustion performance and pollutant emissions analysis using diesel/gasoline/iso-butanol blends in a diesel engine. Energy Conversion and Management. 2017; 149: p. 381-391.
5. Tavlarides LL, Antiescu G, inventors; Supercritical diesel fuel composition, combustion process and fuel system. US patent 7,488,357. 2009.
6. Vogel T, Götz G, Wensing M. Transition of fuel components into supercritical state under diesel process conditions. In Proc 25th ILASS Europe; 2013; Chania.
7. Lemaire R, Faccinetto A, Therssen E, Ziskind M, Focsa C, Desgroux P. Experimental comparison of soot formation in turbulent flames of diesel and surrogate diesel fuels. In Proceedings of the Combustion Institute; 2009.
8. Luning Prak DJ, Alexandre SM, Cowart JS, Trulove PC. Density, viscosity, speed of sound, bulk modulus, surface tension, and flash point of binary mixtures of n-dodecane with 2, 2, 4, 6, 6-pentamethylheptane or 2, 2, 4, 4, 6, 8, 8-heptamethylnonane. Journal of Chemical & Engineering Data. 2014; 59: p. 1334–1346.
9. Nayyar A, Sharma D, Soni SL, Mathur A. Characterization of n-butanol diesel blends on a small size variable compression ratio diesel engine: modeling and experimental investigation.. Energy Conversion and Management. 2017; 150: p. 242-258.
10. Nabi MN, Zare A, Hossain FM, Bodisco TA, Ristovski ZD, Brown RJ. A parametric study on engine performance and emissions with neat diesel and diesel-butanol blends in the 13-Mode European Stationary Cycle. Energy conversion and management. 2017; 148: p. 251-259.
11. Mueller CJ, Cannella WJ, Bruno TJ, Bunting B, Dettman HD, Franz JA, et al. Methodology for formulating diesel surrogate fuels with accurate compositional, ignition-quality, and volatility characteristics. Energy & Fuels. 2012; 26: p. 3284–3303.
12. Luning Prak DJ, Morris RE, Cowart JS, Hamilton LJ, Trulove PC. Density, viscosity, speed of sound, bulk modulus, surface tension, and flash point of Direct Sugar to Hydrocarbon Diesel (DSH-76) and binary mixtures of n-hexadecane and 2, 2, 4, 6, 6-pentamethylheptane. Journal of Chemical & Engineering Data. 2013; 58: p. 3536–3544.
13. Srivastava SP, Hancsok J. Fuels and Fuel-Additives: John Wiley & Sons; 2014.
14. Lemmon EW, Huber ML. Thermodynamic properties of n-dodecane. Energy & Fuels. 2004; 18: p. 960–967.
15. Gieleciak R. GCxGC studies of palette compounds used in the next generation of diesel fuel surrogate blends. ; 2016.
16. Theodorakakos A, Mitroglou N, Atkin C, Gavaises M. Friction-induced heating in nozzle hole micro-channels under extreme fuel pressurisation. FUEL. 2014; 123: p. 143-150.
17. Strotos G, Koukouvinis P, Theodorakakos A, Gavaises M, Bergeles G. Transient heating effects in high pressure Diesel injector nozzles. International Journal of Heat and Fluid Flow. 2015; 51: p. 257–267.
18. Strotos G, Malgarinos I, Nikolopoulos N, Gavaises M. Predicting the evaporation rate of stationary droplets with the VOF methodology for a wide range of ambient temperature conditions. International Journal of Thermal Sciences. .
19. Murali Girija M, Koukouvinis P, Gavaises M. A simultaneous numerical simulation of cavitation and atomization using a fully compressible three-phase model. Physical Review Fluids. 2018.

20. Kolev N. Diesel Fuel Properties. In Multiphase Flow Dynamics 3: Turbulence, Gas Absorption and Release.: Springer; 2002.
21. Lemmon EW, Huber ML, McLinden MO. NIST Reference fluid thermodynamic and transport properties database (REFPROP). 2013..
22. Sudiro M, Bertucco A. roduction of synthetic gasoline and diesel fuel by alternative processes using natural gas and coal: Process simulation and optimization. Energy. 2009; 34: p. 2206–2214.
23. Ely JF, Huber ML. NIST thermophysical properties of hydrocarbon mixtures database (SUPERTRAPP). 2007..
24. Lin R, Tavlarides LL. Thermophysical properties needed for the development of the supercritical diesel combustion technology: Evaluation of diesel fuel surrogate models. The Journal of Supercritical Fluids. 2012; 71: p. 136–146.
25. Stamataki S, Tassios D. Performance of cubic EOS at high pressures. Revue de l'Institut Français du Pétrole. 1998; 53: p. 367–377.
26. Pedersen K, Milter J, Sørensen H. Cubic equations of state applied to HT/HP and highly aromatic fluids. In SPE Annual Technical Conference and Exhibition; 2002.
27. Gross J, Sadowski G. Perturbed-chain SAFT: An equation of state based on a perturbation theory for chain molecules. Industrial & Engineering Chemistry Research. 2001; 40: p. 1244–1260.
28. Kontogeorgis GM, Folas GK. Appendix A. In Thermodynamic models for industrial applications: from classical and advanced mixing rules to association theories.: John Wiley & Sons; 2009.
29. Liang X, Yan W, Thomsen K, Kontogeorgis GM. On petroleum fluid characterization with the PC-SAFT equation of state. Fluid Phase Equilibria. 2014; 375: p. 254–268.
30. Tihic A, Kontogeorgis GM, von Solms N, Michelsen ML, Constantinou L. A predictive group-contribution simplified PC-SAFT equation of state: application to polymer systems. Industrial & Engineering Chemistry Research. 2007; 47: p. 5092–5101.
31. De Villiers A, Schwarz C, Burger A, Kontogeorgis G. Evaluation of the PC-SAFT, SAFT and CPA equations of state in predicting derivative properties of selected non-polar and hydrogen-bonding compounds. Fluid Phase Equilibria. 2013; 338: p. 1–15.
32. Leekumjorn S, Krejbjerg K. Phase behavior of reservoir fluids: Comparisons of PC-SAFT and cubic EOS simulations. Fluid Phase Equilibria. 2013; 359: p. 17–23.
33. Peng DY, Robinson DB. A new two-constant equation of state. Industrial & Engineering Chemistry Fundamentals. 1976; 15: p. 59–64.
34. Soave G. Equilibrium constants from a modified Redlich-Kwong equation of state. Chemical Engineering Science. 1972; 27: p. 1197–1203.
35. Yan W, Varzandeh F, Stenby EH. PVT modeling of reservoir fluids using PC-SAFT EoS and Soave-BWR EoS. Fluid Phase Equilibria. 2015; 386: p. 96-124.
36. Burgess WA, Tapriyal D, Morreale BD, Soong Y, Baled HO, Enick RM, et al. Volume-translated cubic EoS and PC-SAFT density models and a free volume-based viscosity model for hydrocarbons at extreme temperature and pressure conditions. Fluid Phase Equilibria. 2013; 359: p. 38–44.
37. Schou Pedersen K, Hasdbjerg C. PC-SAFT equation of state applied to petroleum reservoir fluids. In SPE Annual Technical Conference and Exhibition; 2007.
38. Gord MF, Roozbahani M, Rahbari HR, Hosseini SJH. Modeling thermodynamic properties of natural gas mixtures using perturbed-chain statistical associating fluid theory. Russian Journal of Applied Chemistry. 2013; 86: p. 867–878.
39. Panuganti SR, Vargas FM, Gonzalez DL, Kurup AS, Chapman WG. PC-SAFT characterization of crude oils and modeling of asphaltene phase behavior. Fuel. 2012; 93: p. 658–669.
40. Zúñiga-Hinojosa MA, Justo-García DN, Aquino-Olivos MA, Román-Ramírez LA, García-Sánchez F. Modeling of asphaltene precipitation from n-alkane diluted heavy oils and bitumens using the PC-SAFT equation of state. Fluid Phase Equilibria. 2014; 376: p. 210–224.
41. Mueller CJ, Cannella WJ, Bays JT, Bruno TJ, DeFabio K, Dettman HD, et al. Diesel surrogate fuels for engine testing and chemical-kinetic modeling: Compositions and properties. Energy & Fuels. 2016; 30:

p. 1445–1461.

42. Puduppakkam K, Naik C, Meeks E, Krenn C, Kroiss R, Gelbmann J, et al. Predictive Combustion and Emissions Simulations for a High Performance Diesel Engine Using a Detailed Fuel Combustion Model. ; 2014.
43. Prediction for Tetradecahydrophenanthrene from Chemspider. [Online]. [cited 2017 May 30. Available from: http://www.chemspider.com/Chemical-Structure.20647.html.
44. Wertheim M. Fluids with highly directional attractive forces. I. Statistical thermodynamics. Journal of Statistical Physics. 1984; 35: p. 19–34.
45. Wertheim M. Fluids with highly directional attractive forces. II. Thermodynamic perturbation theory and integral equations. Journal of Statistical Physics. 1984; 35: p. 35–47.
46. Wertheim M. Fluids with highly directional attractive forces. III. Multiple attraction sites. Journal of Statistical Physics. 1986; 42: p. 459–476.
47. Wertheim M. Fluids with highly directional attractive forces. IV. Equilibrium polymerization. Journal of Statistical Physics. 1986; 42: p. 477–492.
48. Lorentz H. Uber die anwendung des satzes vom virial in der kinetischen theorie der gase. Annalen der Physik. 1881; 248: p. 127–136.
49. Tapriyal D, Enick R, McHugh M, Gamwo I, Morreale B. High Temperature, high pressure equation of state density correlations and viscosity correlations. ; 2012.
50. Justo-García DN, García-Sánchez F, Romero-Martínez A, Díaz-Herrera E, Juaristi E. Isothermal Multiphase Flash Calculations with the PC-SAFT Equation of State. In AIP Conference Proceedings; 2008.
51. Baker LE, Pierce AC, Luks KD. Gibbs energy analysis of phase equilibria. Society of Petroleum Engineers Journal. 1982; 22: p. 731-42.
52. Michelsen ML. The isothermal flash problem. Part I. Stability. Fluid phase equilibria. 1982; 9: p. 1-9.
53. Fletcher R. Unconstrained Optimization Wiley. In Practical Methods of Optimization. Vol. 1.: Wiley Interscience; 1980.
54. Baled HO, Gamwo IK, Enick RM, McHugh MA. Viscosity models for pure hydrocarbons at extreme conditions: A review and comparative study. Fuel. 2018; 218: p. 89–111.
55. Lohrenz J, Bray BG, Clark CR. Calculating viscosities of reservoir fluids from their compositions. Journal of Petroleum Technology. 1964; 16: p. 1171–1176.
56. Quiñones-Cisneros SE, Zéberg-Mikkelsen CK, Fernández J, García J. General friction theory viscosity model for the PC-SAFT equation of state. AIChE Journal. 2006; 52: p. 1600–1610.
57. Llovell F, Marcos R, Vega L. Free-volume theory coupled with soft-SAFT for viscosity calculations: comparison with molecular simulation and experimental data. The Journal of Physical Chemistry B. 2013; 117: p. 8159–8171.
58. Yarranton HW, Satyro MA. Expanded fluid-based viscosity correlation for hydro- carbons. Industrial & Engineering Chemistry Research. 2009; 48: p. 3640–3648.
59. Chung TH, Ajlan M, Lee LL, Starling KE. Generalized multiparameter correlation for nonpolar and polar fluid transport properties. Industrial & Engineering Chemistry Research. 1988; 27: p. 671–679.
60. Pedersen KS, Fredenslund A. An improved corresponding states model for the prediction of oil and gas viscosities and thermal conductivities. Chemical Engineering Science. 1984; 39: p. 1011–1016.
61. Lotgering-Lin O, Gross J. Group contribution method for viscosities based on entropy scaling using the perturbed-chain polar statistical associating fluid theory. Industrial & Engineering Chemistry Research. 2015; 54: p. 7942–7952.
62. Rosenfeld Y. Relation between the transport coefficients and the internal entropy of simple systems. Physical Review A. 1977; 15: p. 2545.
63. Chapman S, Cowling TG. The mathematical theory of non-uniform gases: an account of the kinetic theory of viscosity, thermal conduction and diffusion in gases. ; 1970.
64. Sauer E, Stavrou M, Gross J. Comparison between a homo-and a heterosegmented group contribution approach based on the perturbed-chain polar statistical associating fluid theory equation of state.

Industrial & Engineering Chemistry Research. 2014; 53: p. 14854–14864.

65. Novak LT. Predicting natural gas viscosity with a mixture viscosity model for the entire fluid region. Industrial & Engineering Chemistry Research. 2013; 52: p. 16014–16018.
66. Grunberg L, Nissan AH. Mixture law for viscosity. Nature. 1949; 164: p. 799–800.
67. Schaschke C, Fletcher I, Glen N. Density and viscosity measurement of diesel fuels at combined high pressure and elevated temperature. Processes. 2013; 1: p. 30–48.
68. Poling BE, Prausnitz JM, John Paul O, Reid RC. The properties of gases and liquids New York: McGraw-Hill; 2001.
69. Wu X, Li C, Jia W. An improved viscosity model based on Peng-Robinson equation of state for light hydrocarbon liquids and gases. Fluid Phase Equilibria. 2014; 380: p. 147-151.
70. Rowane AJ. High-Temperature, High-Pressure viscosities and densities of toluene; MS Thesis. ; 2016.
71. American Society for Testing and Materials. Standard specification for diesel fuel oils D975. ; 2011.
72. Bedoya ID, Arrieta AAA, Cadavid F. Effects of mixing system and pilot fuel quality on diesel-biogas dual fuel engine performance. Bioresource Technology. 2009; 100: p. 6624-6629.